

Nonlinear MPC for Quadrotors in Close-Proximity Flight with Neural Network Downwash Prediction

Jinjie Li¹, Liang Han^{2*}, Haoyang Yu², Yuheng Lin², Qingdong Li¹, Zhang Ren¹

Abstract—Swarm aerial robots are required to maintain close proximity to successfully traverse narrow areas in cluttered environments. However, this movement is affected by the downwash effect generated by the other quadrotors in the swarm. This aerodynamic effect is highly nonlinear and hard to model by classic mathematical methods. In addition, the motor speeds of quadrotors are risky to reach the limit when resisting the effect. To solve these problems, we integrate a Neural network Downwash Predictor with Nonlinear Model Predictive Control (NDP-NMPC) to propose a trajectory-tracking approach. The network is trained with spectral normalization to ensure robustness and safety on uncollected cases. The predicted disturbances are then incorporated into the optimization scheme in NMPC, which handles constraints to ensure that the motor speed remains within safe limits. We also design a quadrotor system, identify its parameters, and implement the proposed method onboard. Finally, we conduct an open-loop prediction experiment to verify the safety and effectiveness of the network, and a real-time closed-loop trajectory tracking experiment which demonstrates a 75.37% reduction of tracking error in height under the downwash effect.

I. INTRODUCTION

Advances in swarm robots have attracted significant attention since they can achieve complex tasks impossible for one robot through cooperation and coordination among a group of robots [1]. As one kind of swarm robot, aerial swarm robots differ from ground robots in that each agent in the group can be affected by the strong airflow generated from its upper neighbors, called the downwash effect [2]. When an agent cannot accurately track its trajectory under the airflow disturbances, it could influence other agents in normal flight, thereby amplifying the disturbance until it affects the entire system. As illustrated in Fig. 1, the lower quadrotor with baseline controller is incapable of traversing a narrow gap under the downwash airflow. Thus, dealing with the downwash effect is critical for the flight safety of aerial swarm robots.

As the distances among aerial robots vary, the downwash effect exhibits a corresponding variation in strength, with greater strength observed at shorter distances and weaker effects observed at longer distances. Hence some research [3], [4] treats the quadrotor as a long-vertical-distance ellipsoid,

This work was supported by the Zhejiang Provincial Natural Science Foundation of China under Grant LGG22F030025, the National Natural Science Foundation of China under Grants 61803014, and the Fundamental Research Funds for the Central Universities.

¹J. Li, Q. Li, and Z. Ren are with the School of Automation Science and Electrical Engineering, Beihang University, Beijing, 100191, China {lijinjie, liqingdong, renzhang}@buaa.edu.cn

²L. Han (*Corresponding author), H. Yu, Y. Lin are with the Sino-French Engineer School, Beihang University, Beijing, 100191, China {liang_han, haoyang_yu, linyuheng}@buaa.edu.cn

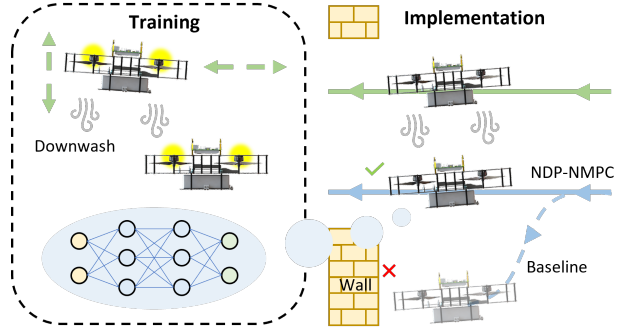


Fig. 1. The core idea of the proposed approach. In training, quadrotors equipped with motor speed sensors collect data for the downwash effect and train a neural network. In the implementation, the proposed method can follow the trajectory under the downwash effect while the baseline is pushed down and cannot pass through a small gap.

attempting to avoid close vertical flight when planning the trajectories. However, this assumption reduces the *reachable set* of the aerial swarm robots, unable to push their mobility into the boundary. A better idea is to regard the downwash effect as a *disturbance rejection* problem and solve it in the control layer [5]. In this way, the planning layer only considers the collision radius of each agent and maximizes the mobility. Therefore, it is necessary to model the downwash disturbance and consider it in the control loop.

The downwash effect is difficult to model by mathematical equations due to its high-degree nonlinearity and fast-changing characteristic. Traditionally, the airflow effect can be accurately modeled through some special flowfield capture devices [6], self-made test benches [7], [8], wind tunnels [9], or Computational Fluid Dynamics (CFD) simulation [10], while these approaches all pose high requirements for experimental equipment or computational time. On the other hand, the rapid development of deep learning in recent years renders the possibility to simulate nonlinear phenomena such as airflow disturbance in low time and fund demands [11]. Shi et al. conducted a series of pioneer research to apply deep learning to model the airflow phenomena in aerial robotics, including the ground effect when the quadrotor lands [12], the downwash disturbances among quadrotors [5], and the disturbances in strong winds [13], which demonstrate the feasibility of modeling downwash effect using neural networks.

When integrating the neural network model inside the control loop, Shi et al. [5] adopted a hierarchical feedback-linearization controller, which generates control input based on only the current states. However, the downwash effect is generated by the relative motions of other quadrotors and

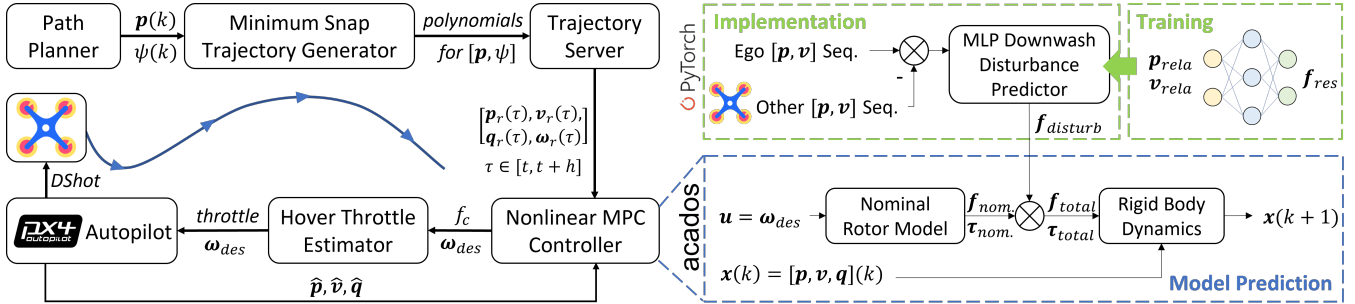


Fig. 2. The overall workflow of the proposed method, which follows the *Path Planning-Trajectory Generation-Control* pipeline. Specifically, Nonlinear Model Predictive Control (NMPC) is adopted for trajectory tracking, of which the model is a nominal quadrotor model added by a predicted disturbance sequence calculated before every iteration. The disturbances are predicted by a neural network from the error state sequence of its own and other quadrotors.

hence can be predicted through the exchange of reference trajectories. If the controller fully exploits this prediction, the overshoots when tracking trajectories will be reduced, which could improve the tracking performance. As a prediction-based method, Model Predictive Control (MPC) can look forward and is a suitable solution to integrate the downwash prediction. Besides, MPC has the advantage of handling constraints [14], which can avoid the motor saturation of quadrotors when resisting disturbances.

Numerous research has attempted to combine deep neural networks with MPC and test the performance of one quadrotor. For example, Salzmann et al. [15] accelerated the computation of a complex neural network using second-order approximations and integrated this simplified network inside the rolling optimization of MPC, which was tested on one single quadrotor. Bauersfeld et al. [16] utilized a physics-network hybrid model to improve the quadrotor model in high-speed flight and combined it with the MPC scheme. Chee et al. [17] attempted to integrate neural ordinary differential equations with MPC and experimented with one Crazyflie quadrotor. In addition, limited research tries to apply this combination to the downwash problem. Matei et al. [18] applied an MPC-based controller with a learning-driven interaction model to solve the downwash problem. Nevertheless, their approach used a neural network as the MPC dynamics to accelerate computation, which is less accurate than a physics-based model and cannot run onboard in real-time.

In this paper, we design a trajectory tracking system in close-proximity flight by integrating a neural network disturbance predictor and Nonlinear Model Predictive Control (NMPC). The proposed approach is inspired by Shi et al. [5] and extends it to NMPC to fully exploit the power of prediction. First, we train a Multilayer Perceptron (MLP) network to predict the disturbance and utilize *spectral normalization* to ensure robustness and generalizability. Then, we synthesize the predictor with NMPC to propose the trajectory tracking method. We also introduce the necessary algorithms to close the loop, including trajectory generation and hover-throttle estimation. Finally, we implement the proposed approach on two quadrotors to verify the effectiveness.

The main contributions are as follows:

- 1) an NMPC-based trajectory tracking method with network disturbance prediction (NDP-NMPC) to integrate the predicted movement information and to solve the saturation constraints under close-proximity flight,
- 2) a hardware system including two quadrotors made from scratch to implement the NDP-NMPC in real-time, and
- 3) open-loop experiments to verify the predictions and closed-loop experiments to test the trajectory tracking effect.

II. METHODOLOGY

This section presents our proposed control scheme with both Nonlinear Model Predictive Control and neural network disturbance observer to enhance the tracking performance in close-proximity flight. First, we present the overall workflow in Section III-A. Then, the coordinate system, notation, and nominal quadrotor model are introduced in Section III-B. Based on these conventions, a neural network observer is implemented to predict the downwash disturbance in Section III-C. Finally, a modified NMPC trajectory tracking controller with disturbance prediction is proposed in Section III-D. We also briefly introduce the generation of the reference trajectory and the estimate of the hover throttle in the final part, which is essential to practical implementation.

A. System Overview

The system architecture is illustrated in Fig. 2. From left to right, a sequence of position points and yaw angles are first sent from a *Path Planner* to a *Trajectory Generator*. The latter module then generates a continuous polynomial trajectory using minimum snap method [19], including multiple derivatives of position and yaw angle. Next, a *Trajectory Server* discretizes the trajectory and calculates the desired full states through differential flatness [19]. These desired full-state points are sent as control reference to an *NMPC Controller* at high frequency to calculate control output. Converted from force to throttle by the *Hover Throttle Estimator*, the control command is eventually executed by a PX4 [20] *Autopilot* to operate the quadrotor. The estimated states are feedback from the *Autopilot* to the *Controller*.

The NMPC controller considers the downwash effect. NMPC is a model-based control approach, and its model

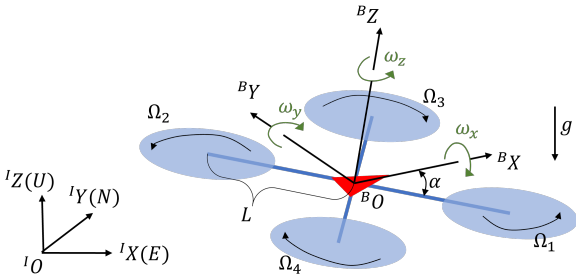


Fig. 3. Diagram of the quadrotor model with the ENU (X East, Y North, Z Up) inertial frame and the FLU (X Forward, Y Left, Z Up) body frame.

consists of two components: one based on a nominal rotor model and the other based on a neural network disturbance predictor. Before a flight, the network is trained to predict disturbance forces based on relative states with the nearby quadrotor. Then, during the flight, the sequence of disturbance prediction is used by the controller to compensate for the downwash effect. By incorporating the downwash effect inside a neural network predictor, the quadrotor can present more accurate trajectory-tracking performance in vertical-aligned flight.

B. Nominal Quadrotor Model

We denote scalars in lowercase $x \in \mathbb{R}$, vectors in bold lowercase $\mathbf{x} \in \mathbb{R}^n$, and matrices in bold uppercase $\mathbf{X} \in \mathbb{R}^{n \times m}$. We use $[\cdot]$ to denote arrays and (\cdot) to denote functions. We use $\hat{\cdot}$ to denote estimated values. The coordinate systems, depicted in Fig. 3, contain the world inertial frame \mathcal{I} , the body frame \mathcal{B} , as well as the propeller numbering convention. The vector in the frame \mathcal{I} is denoted as ${}^I\mathbf{p}$, and the rotation from \mathcal{B} to \mathcal{I} is denoted as ${}^I_B\mathbf{R}$ (rotation matrix) or ${}^I_B\mathbf{q}$ (attitude quaternion). We use the ENU inertial frame and the FLU body frame to be compatible with the MAVROS toolkit, a ROS package to communicate with various autopilots such as PX4.

We use $\mathbf{q} = [q_w, q_x, q_y, q_z]^T \in \mathbb{H}$ to denote the attitude quaternion in *Hamilton-convention* [21], $\mathbf{q}^* = [q_w, -q_x, -q_y, -q_z]^T$ to denote the quaternion conjugation, and \circ to denote the quaternion multiplication operator. The attitude quaternion is a unit quaternion ($\|\mathbf{q}\|=1$), and thus the inverse of quaternion \mathbf{q}^{-1} is the same as \mathbf{q}^* . We use $\mathcal{V}(\cdot)$ to represent the vector part of the quaternion $\mathcal{V}(\mathbf{q}) := [q_x, q_y, q_z]^T, \mathbb{H} \rightarrow \mathbb{R}^3$, and $\mathcal{V}^*(\cdot)$ to denote the reverse mapping from a position point $\mathcal{V}^*(\mathbf{p}) := [0, \mathbf{p}]^T, \mathbb{R}^3 \rightarrow \mathbb{H}$. Then full SE3 transformations from \mathcal{B} to \mathcal{I} can be represented as ${}^I\mathbf{p} = \mathcal{V}({}^I_B\mathbf{q} \circ \mathcal{V}^*({}^B\mathbf{p}) \circ {}^I_B\mathbf{q}^*) + {}^I\mathbf{p}_{Bo} = {}^I_B\mathbf{R}(\mathbf{q}){}^B\mathbf{p} + {}^I\mathbf{p}_{Bo}$, where ${}^I\mathbf{p}_{Bo}$ is the position of \mathcal{B} frame's origin in the \mathcal{I} frame, and $\mathbf{R}(\mathbf{q})$ is the rotation matrix from a quaternion following:

$$\mathbf{R} = \begin{bmatrix} 1 - 2q_y^2 - 2q_z^2 & 2q_xq_y - 2q_wq_z & 2q_xq_z + 2q_wq_y \\ 2q_xq_y + 2q_wq_z & 1 - 2q_x^2 - 2q_z^2 & 2q_yq_z - 2q_wq_x \\ 2q_xq_z - 2q_wq_y & 2q_yq_z + 2q_wq_x & 1 - 2q_x^2 - 2q_y^2 \end{bmatrix}.$$

We assume that the origin of the body frame \mathcal{B} is at the center of mass, and four rotors are all placed in the \mathcal{B} frame's XY-plane. Established from 6-DoF rigid body dynamics, the

quadrotor model is written as follows [14]

$${}^I\dot{\mathbf{p}} = {}^I\mathbf{v}, \quad (1)$$

$${}^I\dot{\mathbf{v}} = ({}^I_B\mathbf{R}(\mathbf{q}) \cdot {}^B\mathbf{f}_u + {}^I\mathbf{f}_d) / m + {}^I\mathbf{g}, \quad (2)$$

$${}^I_B\dot{\mathbf{q}} = 1/2 \cdot {}^I_B\mathbf{q} \circ \mathcal{V}^*({}^B\boldsymbol{\omega}), \quad (3)$$

$${}^B\dot{\boldsymbol{\omega}} = \mathbf{I}^{-1} \cdot (-{}^B\boldsymbol{\omega} \times (\mathbf{I} \cdot {}^B\boldsymbol{\omega}) + {}^B\boldsymbol{\tau}_u + {}^B\boldsymbol{\tau}_d), \quad (4)$$

where m is mass, ${}^I\mathbf{g} = [0, 0, -g]^T$ is gravity vector, $\mathbf{I} = \text{diag}(I_{xx}, I_{yy}, I_{zz})$ is inertia matrix assuming that the quadrotor exhibits symmetry across all three axes, ${}^B\mathbf{f}_u$ and ${}^B\boldsymbol{\tau}_u$ are force and torque caused by the rotors, ${}^I\mathbf{f}_d$ and ${}^B\boldsymbol{\tau}_d$ are force and torque caused by disturbances, and ${}^B\boldsymbol{\omega} = [\omega_x, \omega_y, \omega_z]^T$ is angular rate vector expressed in the body frame.

The thrust generated by rotors is assumed to be vertical to the \mathcal{B} frame's XY-plane, and we therefore obtain ${}^B\mathbf{f}_u = [0, 0, f_c]^T$ and ${}^B\boldsymbol{\tau}_u = [\tau_x, \tau_y, \tau_z]^T$, where f_c is the collective force of four rotors. We use a quadratic fit to model the thrust and torque for each propeller:

$$f_i = k_t \cdot \Omega^2, \quad \tau_i = k_q \cdot \Omega^2, \quad (5)$$

where k_t and k_q are thrust coefficient and torque coefficient, respectively, as well as Ω represents motor speed in kRPM. Then the $[f_c, \tau_x, \tau_y, \tau_z]^T$ and the thrust of each rotor f_i is connected by

$$[f_c, \tau_x, \tau_y, \tau_z]^T = \mathbf{G} \cdot [f_1, f_2, f_3, f_4]^T, \quad (6)$$

in which the control allocation matrix \mathbf{G} is

$$\mathbf{G} = \begin{bmatrix} 1 & 1 & 1 & 1 \\ L \sin \alpha & -L \sin \alpha & -L \sin \alpha & L \sin \alpha \\ -L \cos \alpha & -L \cos \alpha & L \cos \alpha & L \cos \alpha \\ k_q/k_t & -k_q/k_t & k_q/k_t & -k_q/k_t \end{bmatrix}, \quad (7)$$

where L and α are geometric parameters shown in Fig. 3.

The quadrotor nominal model established above is used to design both disturbance observer and controller. The disturbing ${}^I\mathbf{f}_d$ and ${}^B\boldsymbol{\tau}_d$ are estimated in the next part.

C. Neural Network Observer for Downwash Effect

This part introduces a neural network observer to model the disturbance between quadrotors in vertical-aligned flight.

1) *Neural Network Disturbance Observer*: Due to airflow's high nonlinearity and fast-changing property, we apply a neural network (NN) to estimate the disturbances. Specifically, we utilize a Multi-Layer Perceptron (MLP) to observe the disturbances. A trained MLP can be viewed as a mapping function $f(\cdot; \theta) : \mathbb{R}^i \rightarrow \mathbb{R}^o$ from the input tensor \mathbf{x} to the output result \mathbf{y} , where $\theta := \{\mathbf{W}^1, \dots, \mathbf{W}^{H+1}\}$ represents the weight parameters, and H is the number of hidden layers. The element-wise ReLU function $\phi(\mathbf{x}) = \max(0, \mathbf{x})$ is selected as the activation function, and then the MLP network can be written as

$$\mathbf{y} = f(\mathbf{x}; \theta) = \mathbf{W}^{H+1} \cdot \phi(\mathbf{W}^H \cdot \phi(\dots \phi(\mathbf{W}^1 \mathbf{x}))). \quad (8)$$

For the downwash effect, the input variables contain relative states of the ego quadrotor and the other quadrotor

$\mathbf{x} = [{}^I\mathbf{p}_{rela}, {}^I\mathbf{v}_{rela}, {}^I\mathbf{q}_{rela}, {}^B\boldsymbol{\omega}_{rela}]^T$, and the output value is the disturbances $\mathbf{y} = [{}^I\hat{\mathbf{f}}_d, {}^B\hat{\boldsymbol{\tau}}_d]^T$.

2) *Spectral Normalization*: When we collect training data in the experiments, the training set is impossible to cover the entire state space. Hence, the output of the network in those data-uncovered states is critical to flight safety. Spectral normalization has been demonstrated in recent papers [12], [22] that it can enhance the robustness and generalization of neural network and hence be adopted.

The spectral normalization can limit the Lipschitz constant of the network and then raise its robustness and generalizability. The Lipschitz constant of a function $\|f\|_{\text{Lip}}$ is defined as the smallest value M that

$$\|f(\mathbf{x}) - f(\mathbf{x}')\| / \|\mathbf{x} - \mathbf{x}'\| \leq M \quad (9)$$

for any \mathbf{x} and \mathbf{x}' , where $\|\cdot\|$ is the l_2 norm. Mathematically, the Lipschitz constant $\|g(\mathbf{x})\|_{\text{Lip}}$ for any function $g(\mathbf{x})$ is equal to the maximum spectral norm (maximum singular value) $\sigma(\cdot)$ of the function's gradient $\sup_{\mathbf{x}} \sigma(\nabla g(\mathbf{x}))$. We can apply this fact to (8) and then obtain

$$\|f(\mathbf{x})\|_{\text{Lip}} = \sigma \left(\prod_{l=1}^{H+1} \mathbf{W}^l \right) \leq \prod_{l=1}^{H+1} \sigma(\mathbf{W}^l). \quad (10)$$

If the weight matrix \mathbf{W}^l is normalized by the spectral norm $\sigma(\cdot)$ and the scale ratio γ at each training epoch

$$\bar{\mathbf{W}}^l := \gamma \cdot \mathbf{W}^l / \sigma(\mathbf{W}^l), \quad (11)$$

then the Lipschitz constant of the network is constrained as

$$\|f(\mathbf{x})\|_{\text{Lip}} \leq \gamma^{H+1}. \quad (12)$$

The spectral normalization actually limits the change rate of the network's output, making the output more uniform. This uniformity prevents drastic changes in the network output, which is also proved in our subsequent experiments.

3) *Data Acquisition*: In the training phase, it is necessary to collect the real disturbance wrench (force and torque) as the training data. We assume that the physical model is accurate, and then the disturbance wrench can be obtained by subtracting the resultant nominal wrench from the resultant real wrench.

Assuming motor speeds can be measured in the training phase, the resultant nominal wrench is calculated as follows:

$${}^I\mathbf{f}_n = {}^I\mathbf{R}(\mathbf{q}) \cdot {}^B\mathbf{f}_u + m \cdot {}^I\mathbf{g}, \quad {}^B\boldsymbol{\tau}_n = {}^B\boldsymbol{\tau}_u, \quad (13)$$

where ${}^B\mathbf{f}_u$ and ${}^B\boldsymbol{\tau}_u$ come from (5) and (6) given the measured motor speeds Ω_i , as well as ${}^I\mathbf{f}_n$ and ${}^B\mathbf{f}_u$ denote the force and torque calculated by the nominal model.

The resultant real wrench can be obtained by odometry modules. The odometry module of autopilot can provide the estimation of velocity and body rate, and then their derivatives ${}^I\dot{\mathbf{v}}$ and ${}^B\dot{\boldsymbol{\omega}}$ are numerically calculated through the Tustin's method. Then the real resultant wrench on the body is obtained through classical mechanics:

$${}^I\mathbf{f} = m \cdot {}^I\dot{\mathbf{v}}, \quad {}^B\boldsymbol{\tau} = \mathbf{I} \cdot {}^B\dot{\boldsymbol{\omega}}. \quad (14)$$

Finally, the disturbance ${}^I\mathbf{f}_d$ and ${}^B\boldsymbol{\tau}_d$ are attained through

$${}^I\mathbf{f}_d = {}^I\mathbf{f} - {}^I\mathbf{f}_n, \quad {}^B\boldsymbol{\tau}_d = {}^B\boldsymbol{\tau} - {}^B\boldsymbol{\tau}_n. \quad (15)$$

Now input $[{}^I\mathbf{p}_{rela}, {}^I\mathbf{v}_{rela}, {}^I\mathbf{q}_{rela}, {}^B\boldsymbol{\omega}_{rela}]$ and output $[{}^I\mathbf{f}_d, {}^B\boldsymbol{\tau}_d]$ has been constructed for training neural networks.

Remark: The resultant force can also be estimated directly through the inertial measurement unit (IMU), but the noise of this approach is unacceptable. In real flight, we drop ${}^I\mathbf{q}_{rela}$ and ${}^B\boldsymbol{\omega}_{rela}$ since the flight speed is slow and quadrotors remain almost horizontal. ${}^B\boldsymbol{\tau}_d$ is also dropped since PX4 has a body rate controller running at 1kHz, which can compensate for it effectively.

D. Nonlinear MPC with Network Disturbance Prediction

In this subsection, we introduce in detail the proposed NMPC-based trajectory tracking controller. The generation approach of reference trajectory and a Kalman filter to estimate hover throttle are also briefly introduced.

1) *Nonlinear MPC*: During the close-proximity flight, we assume that every quadrotor adopts the NMPC controller, and thus they can exchange predictions with each other, making the prediction of future disturbances available.

Nonlinear MPC is chosen in close-proximity flight because of two reasons. First, the thrust command is highly possible to saturate when the lower quadrotor is influenced by the upper one's downwash airflow, and MPC is powerful for handling saturation. Second, the future trajectory of another quadrotor can be obtained through communication, which helps the ego quadrotor to prepare for the downwash effect in advance.

Given the reference trajectory, the cost function is defined as the error between predicted and reference states in the time horizon. Then a constrained nonlinear optimization problem is formulated as

$$\min_{\mathbf{u}_k} \left(\bar{\mathbf{x}}_N^T \mathbf{Q}_N \bar{\mathbf{x}}_N + \sum_{k=0}^{N-1} (\bar{\mathbf{x}}_k^T \mathbf{Q} \bar{\mathbf{x}}_k + \bar{\mathbf{u}}_k^T \mathbf{R} \bar{\mathbf{u}}_k) \right) \quad (16)$$

with constraints of dynamics, initial values, and control input:

$$\begin{aligned} \mathbf{x}_{k+1} &= f(\mathbf{x}_k, \mathbf{u}_k), \\ \mathbf{x}_0 &= \mathbf{x}_{\text{init}}, \\ \mathbf{u}_k &\in [\mathbf{u}_{\min}, \mathbf{u}_{\max}], \end{aligned} \quad (17)$$

where the symbol $\bar{(\cdot)} = (\cdot) - (\cdot)_r$ denotes the error w.r.t. the reference, \mathbf{Q}_N , \mathbf{Q} , and \mathbf{R} are diagonal matrices representing terminal cost, state cost, and control energy cost, respectively, and $f(\cdot)$ is the quadrotor nominal model (1-3) discretized by the 4-order *Runge-Kutta* method. Specifically, the state is $\mathbf{x}_k = [{}^I\mathbf{p}_k, {}^I\mathbf{v}_k, {}^I\mathbf{q}_k]^T$, and the control input is $\mathbf{u}_k = [f_c, {}^B\boldsymbol{\omega}, {}^I\mathbf{f}_d]^T$. Note that the error of quaternion is $\bar{\mathbf{q}} = \mathcal{V}(\mathbf{q} \circ \mathbf{q}_r^{-1})$, and the input ${}^I\mathbf{f}_d$ is actually a fixed value bounded by ${}^I\mathbf{f}_{d\min} = {}^I\mathbf{f}_{d\max} = {}^I\hat{\mathbf{f}}_d$. Then *Warm-Starting*, *Real-Time Iteration (RTI)*, and *Multi-Shooting* techniques [23] are applied to accelerate the computation. This process is illustrated in Fig. 4, and we refer readers to [14] for

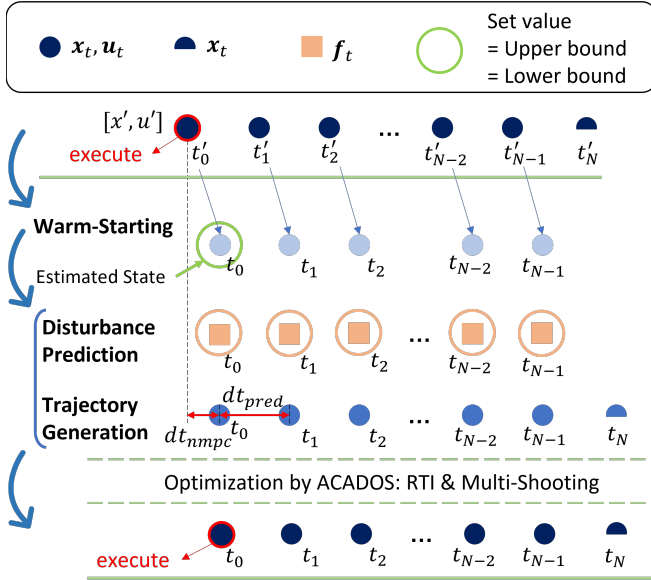


Fig. 4. A diagram to illustrate NDP-NMPC algorithm. From top to bottom, each state point's initial value in this iteration comes from the result of the last iteration, which is called *warm-starting*. Then the first state is constrained to the real state, introducing the feedback mechanism into MPC. Next, the disturbances are predicted by the neural network, and the reference states are provided by the trajectory server. Eventually, these data points are sent to ACADOS [23] for optimization.

more details about the NMPC controller. Finally, the control command is extracted from the optimized result sequence:

$$\mathbf{u}_{\text{NDP-NMPC}} = \mathbf{u}_0^* = [f'_c, \omega'_x, \omega'_y, \omega'_z]. \quad (18)$$

Remark: Note that we drop (4) in the quadrotor nominal model and exclude the τ_d from the input since the PX4 contains a body rate controller working in 1kHz, which provides a quick response for body rate command and can compensate for the disturbance torque τ_d effectively in real flight.

2) *Reference Trajectory Generation*: Trajectory generation refers to generating a smooth, dynamic feasible, and time-indexed curve to pass a set of points, including a start point, several pre-defined waypoints, and an end point. As the quadrotors are mathematically *differential flatness*, the trajectory generation can be converted to a polynomial optimization problem for the four flat output $[x, y, z, \psi]$, which are 3D position and yaw angle. We implement the *minimum snap* algorithm based on [19], except that the time allocation between points is achieved by simply dividing the relative distance by the user-defined average velocity.

The generated trajectory is a set of parametric equations. Therefore, a trajectory server is needed to discretize the curve, choose the future reference states compatible with the prediction horizon of NMPC, and publish these references at a frequency no lower than the control loop.

3) *Hover Throttle Estimate*: The Nonlinear MPC generates the collective thrust and torque as the control input. However, the PX4 autopilot requires the thrust to be normalized into $[0, 1]$. Specifically, we use the hover throttle h_v to normalize it and denote the normalized result (throttle) as h . In actual flight, h_v slowly increases due to the battery

voltage decrease. To accurately estimate the hover throttle, we implement a simple Kalman Filter estimator similar to the PX4 autopilot [24].

The estimator uses $\hat{\mathbf{x}} = [\hat{f}_c, \hat{\gamma}_h]^T$ as the state and $z = {}^B a_{\text{sp},z}$ as the measurement, where \hat{f}_c is the collective force generated by all rotors, $\hat{\gamma}_h := mg/h_v$ is the thrust parameter, and $a_{\text{sp},z}$ is the *specific force* of Z axis measured from the IMU. If we assume that the specific force all comes from the rotors, then the system model and the measurement model can be written as

$$\hat{\mathbf{x}}(k) = \begin{bmatrix} 0 & h(k) \\ 0 & 1 \end{bmatrix} \cdot \hat{\mathbf{x}}(k-1), \quad (19)$$

$$z(k) = \begin{bmatrix} 1 \\ m \end{bmatrix} \cdot \hat{\mathbf{x}}(k). \quad (20)$$

Following the standard equations of Kalman Filter, $\hat{\gamma}_h$ can be identified online during the flight. Finally we normalize the thrust force as $h' = f'_c/\hat{\gamma}_h$ and then feed $[h', \omega'_x, \omega'_y, \omega'_z]$ into the PX4 autopilot.

Remark: Note that the assumption we made neglects all disturbances, and hence the estimation only works when the quadrotors are unaffected by others. In real flight, we update the thrust parameter before trajectory tracking.

III. EXPERIMENTS

In this section, we introduce the setup of experiments and analyze the results. We first present the system identification of hardware platforms, then the data collection of the downwash effect, next an open-loop experiment for disturbance prediction, and finally a closed-loop trajectory tracking experiment to verify the control performance.

A. Hardware and Parameter Identification

To verify the proposed algorithm, we make our flight platform as shown in Fig. 5a. The platform contains a pixhawk 4 autopilot for low-level flight control and state estimation, an NVIDIA TX2 NX for algorithm execution, several passive reflective markers for indoor localization, and other electrical devices essential to flight such as a WIFI module, a receiver, and four ESCs that support rotor speed measurement through the DShot protocol [25].

We follow a similar procedure in [26] to identify the rotor parameters with a load cell, as shown in Fig. 5b. We 3D print

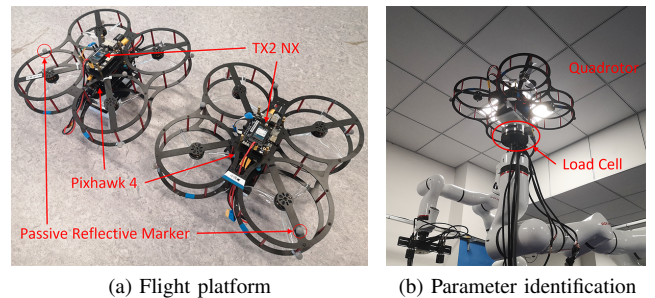


Fig. 5. (a) Two self-made quadrotors with onboard computing resources. (b) The quadrotor is identified for rotor parameters and inertial parameters.

TABLE I
IDENTIFIED PARAMETERS

Parameter(s)	Value(s)	Unit
L	0.1372	m
α	45	deg
m	1.5344	kg
g	9.81	m/s^2
I_{xx}	0.0094	$kg \cdot m^2$
I_{yy}	0.0134	$kg \cdot m^2$
I_{zz}	0.0145	$kg \cdot m^2$
k_q	3.7611 E-4	$N \cdot m/kRPM^2$
k_t	2.8158 E-2	$N/kRPM^2$
$[\Omega_{\min}, \Omega_{\max}]$	[2.6, 24.0]	kRPM
thrust/weight	4.3100	—
flight time	705	s

a connector to place the whole quadrotor on the load cell and give square wave signals to drive a pair of propellers on the diagonal. Compared with only placing one motor on the load cell, this setup considers the body's airflow effect on rotors. We assume that the quadrotor is symmetrical in all three axes, and then the inertial matrix becomes a diagonal matrix, of which the diagonal elements are measured using the bifilar-pendulum method [27]. Identified parameters are listed in Table I. These parameters are used in the PX4 Simulation-In-The-Loop environment to simulate the proposed approach.

B. Data Collection, Learning, and Open-Loop Prediction

Two quadrotors are controlled by pilots to fly over each other to collect data points under the downwash effect. We fix the lower one and move the upper one to raise the possibility of overlapping. The height of the moving quadrotor varies to increase the data diversity. Quadrotors' data, including the state and estimated disturbance with a timestamp, are collected at 100Hz using the ROS tool `rosbag`, and 570-second data are collected in total for both quadrotors. The data can be doubled since the two quadrotors are symmetrical. Then the data are aligned in time, and subtract the average disturbance force in the hover state to remove the bias.

We design a Multilayer Perceptron network with the 6-128-64-128-3 structure, of which the input includes the 3-axis relative position and velocity, as well as the output is the 3-axis disturbance force. Basic parameters for training the network are listed in Table IIa. The network uses the ReLU function as the activation function, Adam [28] as the optimizer, and Mean Squared Error (MSE) as the loss function. The collected data are shuffled, of which 70 percent are selected as the training data. The network is implemented in PyTorch, and the predictions for a sequence of states can be computed once in one batch.

The spectral normalization ratio γ is critical to the balance of accuracy and robustness, which make us execute some experiments to find the best value. We record the losses of different γ in Table IIb, and we plot the predictions in different heights as Fig. 6 to evaluate the performances in the cases where no data is covered. From the table, it is obvious that the loss increases with the decrease of γ , i.e., the stronger the influence of spectral normalization, the less

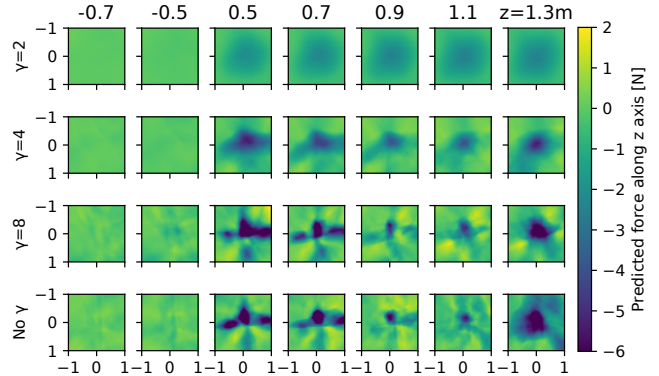


Fig. 6. Disturbance predictions of the neural network under different spectral normalization ratios γ . Each square represents the predicted Z-force in a $1m \times 1m$ X-Y area. We fix the relative velocity to zero and change the γ to observe the output at different heights. The relative heights of the other quadrotor to the ego one are listed from left to right, where the negative numbers indicate flying above. The disturbance predictions for the X and Y axes are not displayed, as they are considered negligible when compared to those of the Z axis.

TABLE II
NEURAL NETWORK PARAMETERS

(a) Training parameters				
Parameter	H	data number	epoch	learning rate
Value	3	57000×2	10000	1e-4
(b) Losses in various spectral normalization ratio γ				
γ	2	4	6	8
Loss	1.6288	1.0523	0.6645	0.6250
				0.6185

accuracy to fit the data. This trend is also observed in Fig. 6, where high γ (the third row) describes the disturbance change with different heights well while low γ (the first row) is too conservative. Nevertheless, this low γ shortage results in a safer prediction on points without data collection. For the third and fourth rows with high γ or without spectral normalization, the predicted force suddenly increases at 1.3m due to the lack of data. However, the first and second rows with Low γ mitigate this trend and guarantee flight safety. Finally, we choose $\gamma = 4$ as the balance of data fitting and safety.

C. Closed-Loop Trajectory Tracking

In this part, we aim to close the loop and verify the feasibility of the proposed method considering hardware limitations such as system delay or limited computing power for embedded platforms. Specifically, we implement the algorithm in python on an onboard TX2 NX computer with control parameters listed in Table III. We fly the quadrotors at a $7 \times 4 \times 3$ room with an OptiTrack motion capture (MoCap) system and utilize the Robot Operation System (ROS) for communication. During the experiment, a PC runs the ROS master node, broadcasts MoCap data, and controls the experimental process. Waypoints for each quadrotor are predefined and used to generate reference trajectories on this PC, which

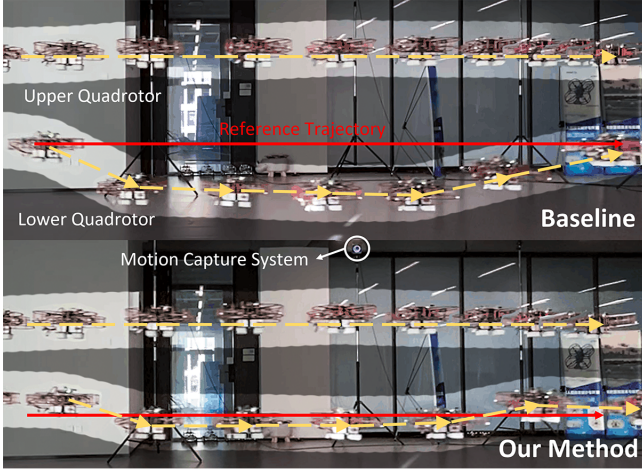


Fig. 7. Comparison of two methods in real-world close-proximity flight. In each scene, two quadrotors are flying together to track the reference trajectories from left to right, and the lower quadrotor suffers from the downwash effect of the upper drone. Note that the camera lens distortion slightly affects the flight trajectories in this figure.

TABLE III
CONTROL PARAMETERS

Parameter	Value	Parameter	Value
N	20	t_{pred}	2s
dt_{nmpc}	1/60s	dt_{pred}	0.1s
$Q_{p,xy}$	300	$Q_{p,z}$	400
$Q_{v,xyz}$	1	$Q_{q,xyz}$	0.1
$R_{\omega,xyz}$	10	R_{f_c}	10

are chosen to ensure an overlapping area (Fig. 8). The NMPC method is implemented using ACADOS for computational acceleration, and the specific control parameters are listed in Table III. We assign high weights to positions as we aim to minimize positional errors.

When conducting an experiment, two quadrotors initiate from the same side but at different heights and proceed to move back and forth. To assess the performance of closed-loop tracking, we conduct several runs and present the real flight scenes and trajectories in Fig. 7 and Fig. 8, respectively. The NMPC method without disturbance prediction [29] is set as the baseline.

From Fig. 8, the baseline quadrotor is severely affected and deviates from the reference. However, the proposed method significantly reduces the impact of disturbances, decreasing the tracking Root-Mean-Square Error (RMSE) by 75.37%, which verifies the effect of the proposed method on the close-proximity flight. We also observe that the lower quadrotor suddenly jumps before it enters the downwash area and then is pushed down to the reference height. This phenomenon is caused by the inaccuracy of neural network predictions. The network predicts a forthcoming disturbance, which ultimately proves to be unfounded, resulting in an unexpected elevation of the lower quadrotor without any corresponding counterbalancing force. This inaccuracy also causes fluctuations on the horizontal plane, which can be observed in Fig. 8. Therefore, the effect of inaccurate predictions must be

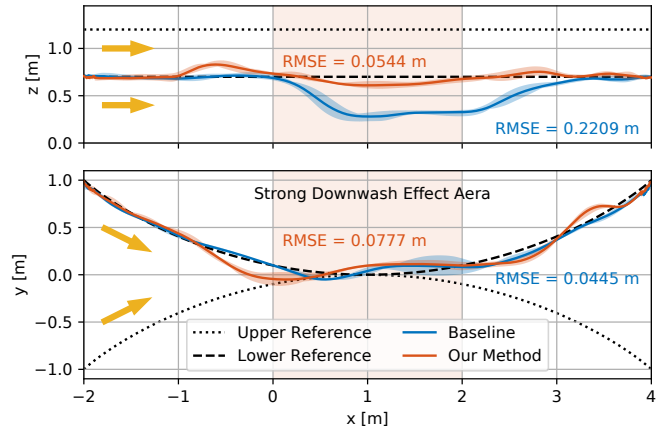


Fig. 8. Comparison of closed-loop tracking results between the baseline [29] and the proposed method. Each curve represents the average of three rounds, with the shaded area indicating the range of values across these rounds. The shaded middle region highlights the zone with a strong downwash effect.

carefully considered when attempting to combine them to improve performance.

IV. CONCLUSION

In this article, we proposed NDP-NMPC, a trajectory tracking method to alleviate the disturbance from downwash airflow in close-proximity flight. This approach utilized a neural network with spectral normalization to predict the disturbances caused by other quadrotors flying above. The network observer was then combined with an NMPC controller. To test the method, we trained a neural network and evaluated the performance of the disturbance prediction. Finally, we executed the algorithm on two quadrotors in real-time for trajectory tracking. We reported that the network was robust to the unseen data, and the proposed approach reduced 75.37% tracking error in the Z axis. In the future, we will extend the proposed method to large-scale swarm drones and consider the uncertainty of predictions in the NMPC workflow.

ACKNOWLEDGMENTS

We thank Dr. Sihao Sun for insightful discussions. We also thank Prof. Qinglei Hu for providing the devices for parameter identification. Finally, we thank Zilu Chen for the mechanical design.

REFERENCES

- [1] X. Zhou, X. Wen, Z. Wang, Y. Gao, H. Li, Q. Wang, T. Yang, H. Lu, Y. Cao, C. Xu, and Fei Gao, "Swarm of micro flying robots in the wild," *Science Robotics*, vol. 7, no. 66, pp. 1–17, May 2022.
- [2] S.-J. Chung, A. A. Paranjape, P. Dames, S. Shen, and V. Kumar, "A Survey on Aerial Swarm Robotics," *IEEE Transactions on Robotics*, vol. 34, no. 4, pp. 837–855, Aug. 2018.
- [3] W. Hönig, J. A. Preiss, T. K. S. Kumar, G. S. Sukhatme, and N. Ayanian, "Trajectory Planning for Quadrotor Swarms," *IEEE Transactions on Robotics*, vol. 34, no. 4, pp. 856–869, Aug. 2018.
- [4] S. H. Arul and D. Manocha, "DCAD: Decentralized Collision Avoidance With Dynamics Constraints for Agile Quadrotor Swarms," *IEEE Robotics and Automation Letters*, vol. 5, no. 2, pp. 1191–1198, Apr. 2020.

[5] G. Shi, W. Hönig, X. Shi, Y. Yue, and S.-J. Chung, "Neural-Swarm2: Planning and Control of Heterogeneous Multirotor Swarms Using Learned Interactions," *IEEE Transactions on Robotics*, vol. 38, no. 2, pp. 1063–1079, Apr. 2021.

[6] D. J. Carter, L. Bouchard, and D. B. Quinn, "Influence of the Ground, Ceiling, and Sidewall on Micro-Quadrotors," *AIAA Journal*, vol. 59, no. 4, pp. 1398–1405, Apr. 2021.

[7] D. Yeo, E. Shrestha, D. A. Paley, and E. M. Atkins, "An Empirical Model of Rotorcraft UAV Downwash for Disturbance Localization and Avoidance," in *Proceedings of AIAA Atmospheric Flight Mechanics Conference*, Jan. 2015, pp. 1–14.

[8] P. Sanchez-Cuevas, G. Heredia, and A. Ollero, "Characterization of the Aerodynamic Ground Effect and Its Influence in Multirotor Control," *International Journal of Aerospace Engineering*, vol. 2017, pp. 1–17, Aug. 2017.

[9] Z. Ma, E. J. Smeur, and G. C. de Croon, "Wind tunnel tests of a wing at all angles of attack," *International Journal of Micro Air Vehicles*, vol. 14, pp. 1–11, Jan. 2022.

[10] A. E. Jimenez-Cano, P. J. Sanchez-Cuevas, P. Grau, A. Ollero, and G. Heredia, "Contact-Based Bridge Inspection Multirotors: Design, Modeling, and Control Considering the Ceiling Effect," *IEEE Robotics and Automation Letters*, vol. 4, no. 4, pp. 3561–3568, Oct. 2019.

[11] J. Willard, X. Jia, S. Xu, M. Steinbach, and V. Kumar, "Integrating scientific knowledge with machine learning for engineering and environmental systems," *ACM Computing Surveys*, vol. 55, no. 4, pp. 1–37, Nov. 2022.

[12] G. Shi, X. Shi, M. O'Connell, R. Yu, K. Azizzadenesheli, A. Anandkumar, Y. Yue, and S.-J. Chung, "Neural Lander: Stable Drone Landing Control Using Learned Dynamics," in *Proceedings of IEEE International Conference on Robotics and Automation*, May 2019, pp. 9784–9790.

[13] M. O'Connell, G. Shi, X. Shi, K. Azizzadenesheli, A. Anandkumar, Y. Yue, and Soon-Jo Chung, "Neural-Fly enables rapid learning for agile flight in strong winds," *Science Robotics*, vol. 7, no. 66, pp. 1–15, May 2022.

[14] S. Sun, A. Romero, P. Foehn, E. Kaufmann, and D. Scaramuzza, "A Comparative Study of Nonlinear MPC and Differential-Flatness-Based Control for Quadrotor Agile Flight," *IEEE Transactions on Robotics*, vol. 38, no. 6, pp. 3357–3373, Dec. 2022.

[15] T. Salzmann, E. Kaufmann, J. Arrizabalaga, M. Pavone, D. Scaramuzza, and M. Ryll, "Real-time neural MPC: Deep learning model predictive control for quadrotors and agile robotic platforms," *IEEE Robotics and Automation Letters*, vol. 8, no. 4, pp. 2397–2404, Feb. 2023.

[16] L. Bauersfeld, E. Kaufmann, P. Foehn, S. Sun, and D. Scaramuzza, "NeuroBEM: Hybrid Aerodynamic Quadrotor Model," in *Proceedings of Robotics: Science and Systems XVII*, Jul. 2021, p. 42.

[17] K. Y. Chee, T. Z. Jiahao, and M. A. Hsieh, "KNODE-MPC: A Knowledge-Based Data-Driven Predictive Control Framework for Aerial Robots," *IEEE Robotics and Automation Letters*, vol. 7, no. 2, pp. 2819–2826, Apr. 2022.

[18] I. Matei, C. Zeng, S. Chowdhury, R. Rai, and J. de Kleer, "Controlling Draft Interactions Between Quadcopter Unmanned Aerial Vehicles with Physics-aware Modeling," *Journal of Intelligent & Robotic Systems*, vol. 101, no. 1, pp. 1–21, Jan. 2021.

[19] D. Mellinger and V. Kumar, "Minimum Snap Trajectory Generation and Control for Quadrotors," in *Proceedings of IEEE International Conference on Robotics and Automation*, May 2011, pp. 2520–2525.

[20] L. Meier, D. Honegger, and M. Pollefeys, "PX4: A node-based multithreaded open source robotics framework for deeply embedded platforms," in *Proceedings of IEEE International Conference on Robotics and Automation*, May 2015, pp. 6235–6240.

[21] H. Sommer, I. Gilitschenski, M. Bloesch, S. Weiss, R. Siegwart, and J. Nieto, "Why and How to Avoid the Flipped Quaternion Multiplication," *Aerospace*, vol. 5, no. 3, pp. 1–15, Sep. 2018.

[22] T. Miyata, T. Kataoka, M. Koyama, and Y. Yoshida, "Spectral Normalization for Generative Adversarial Networks," in *Proceedings of International Conference on Learning Representations*, Feb. 2018, pp. 1–14.

[23] R. Verschueren, G. Frison, D. Kouzoupis, J. Frey, N. v. Duijkeren, A. Zanelli, B. Novoselnik, T. Albin, R. Quirynen, and M. Diehl, "acados—a modular open-source framework for fast embedded optimal control," *Mathematical Programming Computation*, vol. 14, no. 1, pp. 147–183, Mar. 2022.

[24] M. Grob, "Quaternion based Estimation and Control for Attitude Tracking of a Quadcopter using IMU sensors," Master's thesis, ETH Zürich, Zürich, Switzerland, Sep. 2016.

[25] "DShot ESCs | PX4 User Guide." [Online]. Available: <https://docs.px4.io/main/en/peripherals/dshot.html>

[26] J. Förster, "System Identification of the Crazyflie 2.0 Nano Quadcopter," Bachelor's thesis, ETH Zürich, Zürich, Switzerland, Aug. 2015.

[27] M. R. Jardin and E. R. Mueller, "Optimized Measurements of Unmanned-Air-Vehicle Mass Moment of Inertia with a Bifilar Pendulum," *Journal of Aircraft*, vol. 46, no. 3, pp. 763–775, May 2009.

[28] D. P. Kingma and J. Ba, "Adam: A Method for Stochastic Optimization," in *Proceedings of International Conference for Learning Representations*, May 2015, pp. 1–11.

[29] D. Falanga, P. Foehn, P. Lu, and D. Scaramuzza, "PAMPC: Perception-Aware Model Predictive Control for Quadrotors," in *Proceedings of IEEE/RSJ International Conference on Intelligent Robots and Systems*, Oct. 2018, pp. 1–8.